Imaging Symmetry-Selected Corner Plasmon Modes in Penta-Twinned Crystalline Ag Nanowires

Mingxia Song,[†] Alexandre Bouhelier,[†] Pierre Bramant,[†] Jadab Sharma,[‡] Erik Dujardin,[‡] Douguo Zhang,[§] and Gérard Colas-des-Francs[†,*]

[†]Laboratoire Interdisciplinaire Carnot de Bourgogne, CNRS UMR 5209, Université de Bourgogne, 9 Avenue Alain Savary, Dijon, France, [‡]CEMES CNRS UPR, 8011 Toulouse, France, and [§]Department of Optics and Optical Engineering, University of Science and Technology of China, Hefei, People's Republic of China

ABSTRACT Using dual-plane leakage radiation microscopy, we investigate plasmon propagation in individual penta-twinned crystalline silver nanowires. By measuring the wavevector content of the light emitted in the substrate, we unambiguously determine the effective index and the losses of the mode propagating in these structures. The experimental results, in particular, the unexpectedly low effective index, reveal the direct influence of the nanowire crystallinity and pentagonal structure on the observed plasmon modes. By analogy with molecular orbitals of similar symmetry, the plasmon modes are also determined numerically in good agreement with the observed values. We further investigate the effect of wire geometry (length, diameter) on the effective index and propagation loss. Our results show that, beyond dissipation concerns, the morphological and structural control obtained in crystalline colloidal plasmonic nanostructures can be exploited to finely tune their optical properties.

KEYWORDS: surface plasmon · silver nanowire · leakage microscopy · Fourier imaging · mode symmetry

Since the pioneering theoretical works of Takahara and Weeber,[1,2] and the experimental demonstration by Dickson and Lyon,[3] the propagation of light in metal nanowires has been the subject of an intense research effort. These one-dimensional structures possess unique propagation characteristics of surface plasmon (SP) modes that are required for the integration of miniaturized optical interconnects,[4] for the development of advanced devices[5] and complex routing architecture.[6−9] Photon coupling to the nanowire SP mode, a potentially limiting factor in practical devices, has been addressed by several strategies including total internal reflection,[3] adapted butt-coupling technique,[10] scattering at wire terminations[6,11] and at adjacent antenna-like structures,[12−14] or by coupling of fluorescent species.[15,16] The out-coupling of the SP mode into free-space photons was also investigated, emphasizing the role of the termination shape on the polarization characteristics[17] and the directionality of the emission diagram.[18,19]

Chemically synthesized crystalline Au or Ag nanowires are usually the preferred materials since they present lower Joule losses compared to lithographed amorphous structures obtained by metal evaporation.[11] However, although these metal nanowires naturally crystallize with five-fold symmetry,[20] their supported plasmon modes are always discussed assuming a circular cross section. We investigate here the effect of wire morphology on the guided SP.

Because of the strong confinement of the mode at the surface of the wire, the observation of plasmon propagation required either near-field imaging,[11,14,21] photoemission electron microscopy,[22] or indirect mapping of polymer fluorescence.[23] Reflection at the end faces and Fabry-Pérot effect were used to estimate the surface plasmon wavelength of the near-field detected modes.[11,21] These technically challenging measurements are well-suited for strongly bound modes in thin nanowires with diameter $D < 100$ nm characterized by short propagation lengths.[1,24] However, when longer propagation lengths are required as in optical interconnects, we propose an alternative approach to directly measure the effective indices of the relevant mode propagating in thicker silver nanowires. The direct measurement of the propagation constant is critically important to fully understand the details of SP propagation in these one-dimensional metal waveguides.

Therefore, we have developed a detection scheme relying on a radiation-loss mechanism of the SP mode occurring when a thick nanowire is deposited on a glass surface. We demonstrate the presence of higher-order modes for crystalline nanowires with pentagonal cross section and measure their propagation properties as the nanowire dimensions vary.

* Address correspondence to gerard.colas-des-francs@u-bourgogne.fr.

Received for review May 5, 2011 and accepted June 17, 2011.

Published online June 18, 2011
10.1021/nn201648d

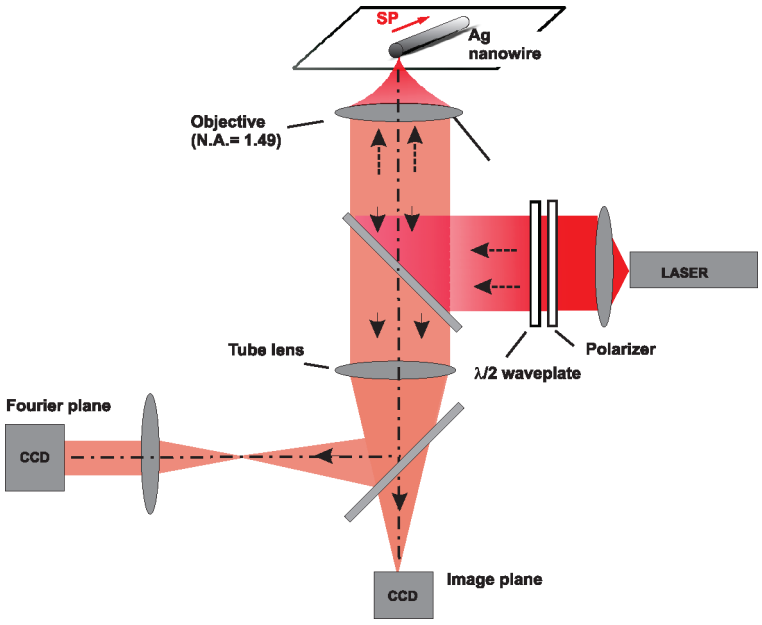

Figure 1. Setup of leakage radiation microscopy of surface plasmon mode propagating in the nanowire. A laser beam is focused at one end of the nanowire by a high numerical aperture objective. Scattering at the extremity insures the excitation of a SP mode in the nanowire. The radiation losses of SP coupled in the substrate are collected by the same objective and are recorded in secondary image and Fourier planes.

RESULTS AND DISCUSSION

The presence of the underlying high-index medium fulfills the phase-matching condition for a decoupling of the SP mode into photons that are radiating in the substrate. Collection of these leakages with a high numerical aperture oil-immersion objective[25−27] and subsequent recording of the image and Fourier conjugated planes of the microscope provide information about the SP intensity[28] and wavevector distributions, respectively.[29,30] The principles of leakage detection of surface plasmons are described in Figure 1. The excitation of the surface plasmon mode is obtained by scattering the diffraction-limited focal spot at the proximal nanowire tip.[11] Light emission from the other end and leakage radiation of the plasmon mode during propagation are collected by the same objective lens and imaged on two CCD cameras, respectively, conjugated with the image and Fourier planes of the microscope.

Silver nanowires were synthesized by a modified protocol based on the polyol process.[31] In general, the polyol method produces nanowires with diameters below 100 nm, which is too restrictive for our optical setup. Therefore, some adjustments of the synthesis protocol were implemented to adjust the nanowires' length and diameter.[32]

In all of our optical experiments, the crystalline Ag nanowires were deposited by drop-casting on glass substrates bearing a grid landmark pattern. Wide-field optical imaging and a piezoelectric translation stage were used to position the wire termination within the diffraction-limited focus of the inverted microscope. Figure 2a displays an image of a selected nanowire (arrow) placed next to an alignment mark. Scanning electron microscopy (SEM) was systematically used to measure the geometrical dimensions of selected nanowires. Figure 2b is a SEM image of the nanowire observed in Figure 2a. A close-up view of its right extremity is displayed in Figure 2c, emphasizing the pentagonal profile of the synthesized crystalline nanowires. For the sake of simplicity, we define the diagonal length of the pentagon as the diameter of the structure.

By optically exciting the Ag nanowire at one extremity with the focal spot, a bright emission spot is usually observed at the distal end, indicating that light transport along the nanowire is taking place.[3] For thin nanowires, the effective index of the SP mode is higher than the index of the substrate and light emission is only observed through a scattering process mediated by the end facets. For thicker wires, however, the visualization of the propagation becomes visible because the wavevector of the mode is contained inside the light cone of the substrate. Figure 3a displays this situation for a $L = 10\ \mu$m long wire with a diameter of $D = 320$ nm. The image represents the intensity distribution measured by a CCD placed in the image plane of the microscope and for a polarization oriented along the nanowire at an excitation wavelength $\lambda = 800$ nm. The focal spot, exciting one end of the wire, appears as a saturated region in the image. Leakage radiations of the surface plasmon mode propagating along the wire are visible in the form of two luminous lines located on either side of the structure. These lines are reminiscent

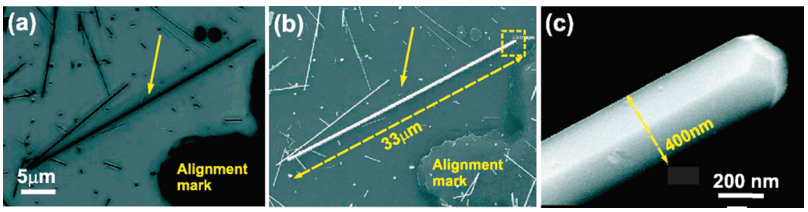

Figure 2. Nanowires are characterized by bright-field optical and scanning electron microscopies (SEM). (a) Bright-field image of a selected 33 μm long nanowire with a width of 400 nm (arrow). (b) SEM image of the same nanowire. (c) High-resolution SEM image of the nanowire termination. The pentagonal cross section is readily visible.

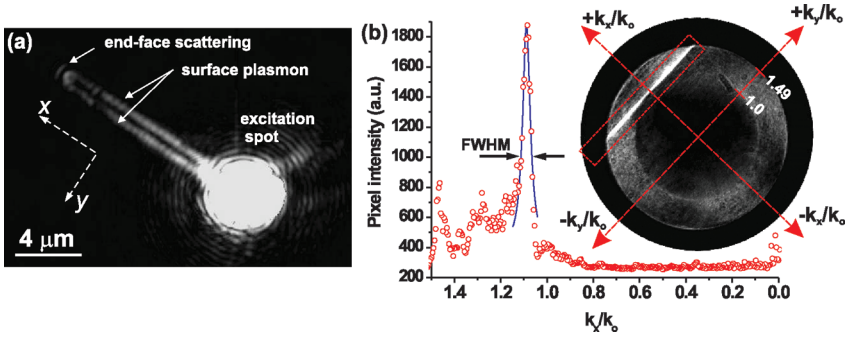

Figure 3. Visualization of the surface plasmon mode in an individual Ag nanowire by leakage radiation microscopy. (a) Intensity distribution in the image plane showing the excitation spot (saturated area), the SP mode along the wire, and its scattering at the extremity. The reference frame is taken along the nanowire (*x*-axis). The excitation wavelength is 780 nm, and the incident linear polarization is aligned with the nanowire. (b) Wavevector distribution obtained by Fourier imaging. The SP mode is recognized as a bright line at a constant k_x/k_o value, here 1.05 (box); $n_{eff}^{max} = 1.49$ and $n_c = 1$ are given by the numerical aperture of the objective and the critical angle, respectively. A cross section along the $+k_x/k_o$ axis is also displayed (red dots). The blue solid line is a Lorentzian fit to the data used to extract the full width at half-maximum (fwhm) of the distribution.

of the intensity distribution at the edges of the nanowire (see below). The observation of these two parallel lines strongly relies on the precise adjustment of the objective correction collar. The reference frame along the nanowire is defined as the *x*-axis.

The wavevector content of the light leaking in the substrate was analyzed by Fourier plane analysis. A typical Fourier plane image is displayed in Figure 3b and represents the projected angular distribution on the plane of the interface. The numerical aperture of the objective (1.49) imposes an upper limit on the collection angle and the measurable effective index n_{eff}^{max}. Because the incident light is focused on a glass/air interface and the entrance pupil of the objective is completely filled, the critical angle is readily observed in the Fourier plane image at $n_c = 1$. The SP mode is recognized as a relatively bright line crossing the plane. The line exhibits a constant but unexpectedly low index along the reciprocal $+k_x/k_o$ axis at 1.05, where $k_o = 2\pi/\lambda$ is the free-space wavevector. Figure 3b also shows a cross section of the Fourier plane along the $+k_x/k_o$ (red dots). The distribution around the bright line is accurately described by a Lorentzian curve[33] (blue solid line) from which the fwhm encoding the losses can be inferred. Here the fwhm is 0.04. The wavevector content along the perpendicular axis k_y/k_o completely fills the detection window, indicating a strong confinement along the *y*-direction expected for a one-dimensional waveguide.[30] In none of the measurements, a diametrically opposed weaker line has been observed which would indicate a plasmon mode running backward at $-k_x/k_o$. We therefore conclude that the reflection coefficient at the end face is low and the energy must be efficiently scattered out. This observation confirms the results concerning the unidirectionality of the emission reported by Shegai *et al.*[19]

The unexpected low value of the effective index of the surface plasmon mode could be accounted for by considering a Ag nanowire with a pentagonal cross section. We numerically investigated the different modes existing in a pentagonal Ag nanowire. Numerical simulations were computed using COMSOL Multiphysics and were cross-checked with a homemade mode solver based on Green's dyad computation.[33,34] Although time-consuming, the latter can easily treat leaky modes in the presence of a substrate.

The modes existing in a pentagonal silver nanowire were first identified by considering a nanowire embedded in a homogeneous background of optical index $n = 1.25$ that roughly mimicks the glass ($n = 1.5$)/air ($n = 1$) interface. The pentagonal nanowires support five modes resulting from a coupling of corner modes[35] which were simulated by using an excitation wavelength $\lambda = 800$ nm and silver optical index $n_{Ag} = 0.0362 + i5.4$.[36] Interestingly, we found that the guided modes displayed in Figure 4a

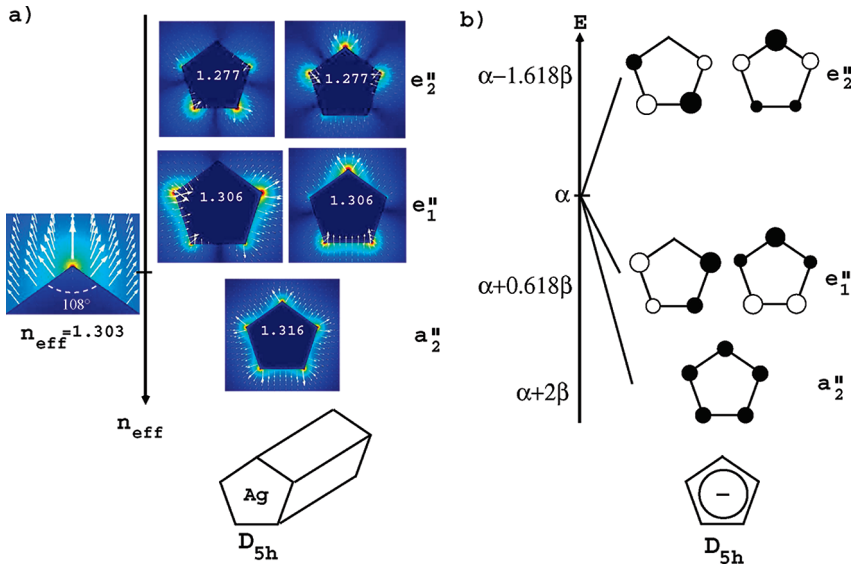

Figure 4. Comparison of the plasmon modes of a pentagonal nanowire with the molecular orbitals of cyclopentadienyl. (a) Intensity profile of an isolated silver corner. When combined to form a pentagonal section, the interaction between the five corners creates mode symmetries in analogy with the molecular orbitals. The wire diameter is 1.25 μm embedded in a medium of optical index n = 1.25. (b) Schematic of the orbital configuration of the molecule displaying a D_{5h} symmetry. The weight and relative signs of the atomic orbital are depicted by the circle area and color (white = positive, black = negative); α is the energy of an isolated atomic π orbital, and β (<0) refers to the coupling strength between orbitals of two adjacent carbons; e''_2, e''_1, and a''_2 are the corresponding Mulliken's symbols.

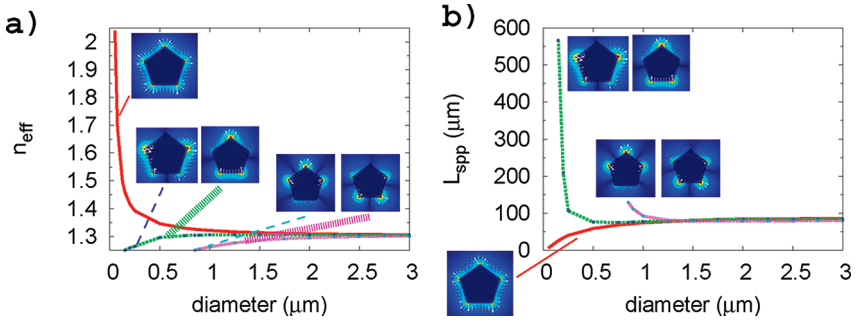

Figure 5. (a) Dispersion of the effective index of the identified modes as a function of wire diameter. The fundamental mode diverges for thin nanowires. The higher-order modes exhibit a cutoff behavior when their effective indices approach the refractive index of the surrounding medium (1.25). (b) Calculated propagation length as a function of wire diameter. The fundamental mode exhibits a high damping for small diameters due to its diverging effective index.

can be described as a linear combination of the five corner modes with weight and polarization strictly analogous to the molecular orbitals of another D_{5h} symmetry system, the cyclopentadienyl molecule. The molecular orbitals of the π-bonds of cyclopentadienyl, deduced from simple Huckel theory, are shown in Figure 4b. Following the conventional representation of molecular orbitals, the weight and relative signs of the atomic orbital in the represented molecular orbital are depicted by the circle area and color (white = positive, black = negative), respectively; α is the energy of an isolated atomic orbital, and β refers to the coupling strength between orbitals of two adjacent carbon atoms. By analogy, the symmetry groups were assigned to the plasmon modes using Mulliken's symbols.

Figure 5a reproduces the dispersion of the effective indices of the five bound modes as a function of the diameter. The radial fundamental mode has no cutoff, similarly to the fundamental TM_0 mode of a circular metallic wire, featuring a divergent effective index for low diameters.[1] The four other guided modes separate in two groups of degenerated modes e''_2 and e''_1 characterized by low effective indices close to the surrounding medium (1.25). These modes run into cutoff at a diameter of about 850 and 150 nm, respectively. Furthermore, we have calculated the dispersion of propagation length L_{spp} of the identified modes in Figure 5b. Close to their cutoff conditions, these modes have a significant longer propagation length that may be suitable for short-scale optical interconnects. Due to their large cutoff diameter, the two degenerated highest modes e''_2 are not of interest for the diameter experimentally investigated and will not be considered further.

Surprisingly, the experimental value of the effective index of the SP mode (n_{eff} = 1.05) is significantly lower than the effective index calculated for a homogeneous medium. In order to account quantitatively for this observation, we introduce the glass substrate in our model. The sample symmetry is then reduced from D_{5h} to C_{2v}, and the modes are no longer degenerated as shown in Figure 6. The fundamental mode remains a bound mode (n_{eff} > 1.5), with the field confined in the high index medium (substrate). Its propagation length is only slightly modified; for a 200 nm diameter, it increases from L_{spp} = 34 μm in a homogeneous background of optical index n = 1.25 to L_{spp} = 48 μm for a glass/air interface. The two others modes become leaky into the substrate (n_{eff} < 1.5) and could therefore be detected using our leakage radiation microscope setup.

In all of the wires studied (total of 42), we have only detected the low effective index mode and were not able to measure the mode expected at n_{eff} = 1.15. We attribute this to a low excitation cross section since this mode appears to be extremely weak in the numerical simulations. Importantly, the measured effective index is in good agreement with the calculated mode at n_{eff} = 1.03. This mode is mainly confined in the low index medium (air), and its effective index only slightly varies for diameters in the range of 100 < D < 250 nm, as shown by the graphs in Figure 7. The effective indices and fwhm for six nanowires with similar lengths (4.8 μm < L < 5.5 μm) but varying diameter were extracted from Fourier plane measurements. Within the considered diameter range, the dispersion is flat and the fwhm of the mode, encoded in the error bar, is constant. The calculated data (open circles) confirm that the effective index is not significantly affected by the diameter of the wire in the considered range. A small discrepancy between the experimental and calculated data remains and can be attributed to the dielectric constant used, the presence of the PVP polymer on the surface of the nanowire, and experimental errors in calibrating Fourier planes.

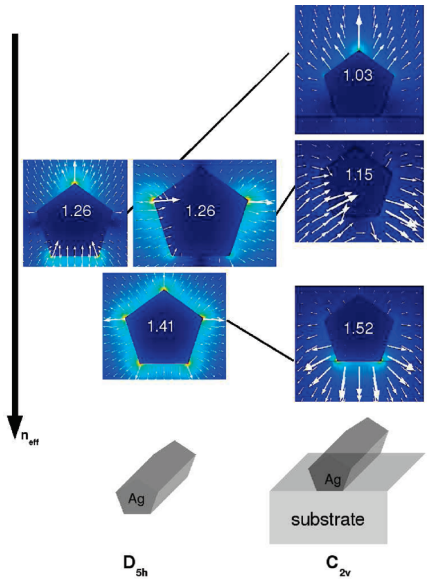

Figure 6. Effect of the substrate on the intensity distribution and effective indices of the SPP guided modes supported by the pentagonal silver wire. The group symmetry is reduced from D_{5h} to C_{2v} so the two degenerated modes at n_{eff} = 1.26 are evolving into two distinct modes at n_{eff} = 1.03 and 1.15. The intensity level for the n_{eff} = 1.15 mode is significantly weaker than the more pronounced n_{eff} = 1.03 mode, suggesting that this mode is inactive. The wire diameter is 200 nm.

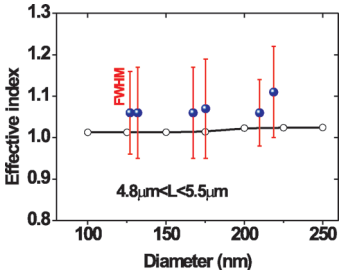

Figure 7. Dispersion curve of the detected mode with nanowire diameter. The experimental data points (filled circles) are extracted from Fourier plane images for nanowires with length 4.8 μm < L < 5.5 μm. The fwhm of the Fourier signature is encoded in the error bars. The open circles are calculated indices.

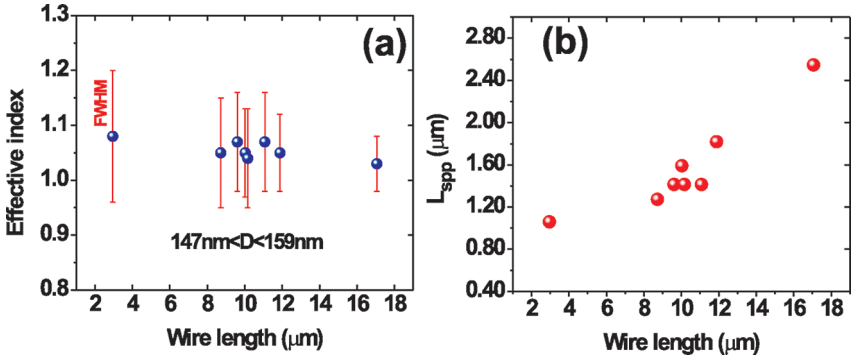

Figure 8. (a) Effective index as a function of lengths for nanowires with a restricted range of diameters. The error bars represent the fwhm of the line measured in the Fourier plane. (b) Inferred propagation length of the SP mode.

In addition to the degeneracy lift, the presence of the substrate strongly modifies the mode propagation length. In a homogeneous background, the two degenerated modes have a high propagation length L_{spp} = 209 μm since they are mainly confined in the dielectric medium. The presence of the substrate introduces a new decay channel through radiation leakage, so that their calculated propagation lengths strongly decrease to L_{spp} = 11.6 μm (n_{eff} = 1.15) or L_{spp} = 5.3 μm (n_{eff} = 1.03) for a nanowire with D = 200 nm.

Since the SP is efficiently scattered at the nanowire distal tip, the fwhm of the mode measured in the Fourier plane should be affected by the nanowire length. In Figure 8a, we plot the experimental value of n_{eff} for different nanowire lengths. For the sake of comparison, we have selected a restricted range of wire diameter composed between 147 and 159 nm. Figure 8a reveals that the effective index can be considered constant within the considered length range. In contrast, the mode fwhm, which is represented by the error bars, is reduced when the length of the wire is increased. The propagation length of the SP mode can be directly inferred from the measure of the fwhm[33] using the relation $L_{spp} = (k_o \times \text{fwhm})^{-1}$. The length dependence of L_{spp} is displayed in Figure 8b, demonstrating that the plasmon propagation length is affected by the length of the nanowire. Distal face scattering is therefore playing a determinant role by introducing an additional decay mechanism, especially for the short nanowires.

CONCLUSIONS

To conclude, we have developed an imaging technique capable of visualizing directly the propagation of surface plasmons in pentagonal crystalline silver nanowires by detecting their leakage radiation. By measuring the lateral and angular intensity distribution of the leakages, the effective indices of the plasmon modes can be experimentally determined. Symmetry considerations derived from an analogy with the well-established molecular orbitals of cyclopentadienyl allowed us to identify the modes existing in the crystalline Ag nanowire with a pentagonal cross section. The role of the substrate on the effective index values of the coupled corner plasmon modes was emphasized, and we have obtained a good agreement with the experimental values. It therefore appears that the precise morphological and structural features of crystalline colloidal metallic nanowires directly contribute to the design of the active plasmon modes, which opens a way to tune the optical properties of these nanostructures beyond the capabilities of lithographically fabricated devices. Finally, we have experimentally shown that distal tip scattering is introducing an additional decay channel contributing to the attenuation of the plasmon propagation. This observation suggests that a better control of the terminal facets of crystalline nanowires is desired in order to tune the tip scattering, which is a future challenge for colloidal chemists.

METHODS

Numerical Simulations. The guided SPs supported by Ag wire were numerically investigated using either commercial (COMSOL Multiphysics, RF module) or homemade (Green's dyad) mode solvers. To this aim, we first considered infinitely long (2D) metallic wires with a pentagonal cross section of various diameters embedded in a homogeneous background (Figure 4 and Figure 5). COMSOL Multiphysics software is a based on finite element method so that both the wire and its surroundings need to be discretized. We used a circular computational window large enough to ensure convergency within a reasonable computing time (between 1.5 and 10 μm) and imposed perfect electric conductor conditions at its boundary. To closely follow the experimental geometry and limit numerical difficulties, the pentagon corners were rounded with a radius of curvature of 5 nm. The whole geometry (wire and surroundings) was discretized using between 20 000 and 60 000 triangular meshes. The homemade mode solver based on 2D Green's dyad computation is described in detail elsewhere.[33,34] It only necessitates discretization of the metallic wire so that the infinitely extended surrounding is naturally taken into account. We used rectangular meshes and cross-checked the obtained effective indices with the values obtained using COMSOL software. Second, we considered wires deposited on a substrate. Green's dyad method easily takes into account leaky modes existing in this configuration, although it is time-consuming. On the contrary, investigating leaky modes using COMSOL software is a difficult task since a phase matching layer (PML) was included to avoid field reflections at the computational window boundaries. Therefore, we used the Green's dyad method to evaluate leaky mode effective indices for typical wire diameters and then determined the optimal PML parameters (thickness and position) required in COMSOL software to ensure convergency (Figure 6). Finally, the two mode solvers give access to a complex effective index of the guided mode, $\tilde{n_{eff}} = n_{eff} + i\, n''_{eff}$ from which the mode propagation length follows $L_{spp} = \lambda_0/4\pi n''_{eff}$.

Ag Nanowire Synthesis. A solution of 1 mM H_2PtCl_6 in 5 mL of ethylene glycol was refluxed for 1 h under refluxing conditions at 150 °C and constant stirring in a 100 mL three-necked round-bottom flask. Once the Pt seed particles were formed, two solutions of 5 mL of $AgNO_3$ (76.5 mM) and 5 mL of polyvinylpyrrolidone (PVP, M_W = 55 000, 0.2 g) in ethylene glycol were added slowly and simultaneously to the reaction flask using two separate dropping funnels. Temperature and stirring rate were adjusted to 165 °C and 600 rpm, respectively, prior to the addition of silver salt and polymer. Reaction was continued for 1 h after addition and followed by cooling to room temperature. The reaction flask was performed under argon flow throughout the reaction to avoid oxide formation. The Ag nanowires were separated from other particle byproducts by careful centrifugation after adding an excess amount of acetone. This purification step was repeated three times, and nanowires were finally dispersed in 30 mL of ethanol and stored in a refrigerator for future use.

Leakage Radiation Microscopy. The leakage microscope was retrofitted on a Nikon TE2000 inverted base. A tunable CW Ti:sapphire (750−830 nm) laser beam was coupled into the epi-port of the microscope with a diameter completely filling the entrance pupil of a high numerical aperture objective (100×, NA = 1.49, Plan-Apo). The polarization state of the excitation was controlled by a

combination of a polarizer and a half-wave plate. The light was focused on a diffraction-limited spot at one end of a nanowire. A combination of relay lenses adjusted at the exit port of the microscope provided a set of imaging planes conjugated either with the field plane (object) or with the aperture plane (Fourier) of the microscope. A CCD camera (Luca from Andor) recorded the intensity distributions in the respective planes. The calibration of the Fourier plane was obtained by combining the known value of the numerical aperture of the objective and the critical angle at the glass/air interface. The images were acquired without any aperture or field stops.[19]

Structural Characterization. Scanning electron microscopy (SEM) was carried out on a JEOL 6500 at an acceleration voltage of 20 kV. The SEM imaging was performed after optical characterization to limit the carbon contamination of the crystalline nanowire. High-magnification view of the synthesized Ag nanowires revealed the pentagonal section of structures.

Acknowledgment. M.S. acknowledges a stipend from the Chinese Scholarship Council. A.B. and G.C.D.F thank the Agence Nationale de la Recherche (ANR) under Grants Plastips (ANR-09-BLAN-0049-01) and the NanoSci E+ program under Grant E^2-PLAS (ANR-08-NSCI-007). E.D. and J.S. acknowledge the financial support of the European Research Council (Grant ERC-2007-StG No. 203872-COMOSYEL), and D.Z. thanks the National Natural Science Foundation of China for Grant No. 11004182.

REFERENCES AND NOTES

1. Takahara, J.; Yamagishi, S.; Taki, H.; Morimoto, A.; Kobayashi, T. Guiding of a One-Dimensional Optical Beam with Nanometer Diameter. *Opt. Lett.* **1997**, *22*, 475.
2. Weeber, J.-C; Dereux, A.; Girard, C.; Krenn, J.; Goudonnet, J.-P. Plasmon Polaritons of Metallic Nanowires for Controlling Submicron Propagation of Light. *Phys. Rev. B* **1999**, *60*, 9061.
3. Dickson, R. M.; Lyon, L. A. Unidirectional Plasmon Propagation in Metallic Nanowires. *J. Phys. Chem. B* **2000**, *104*, 6095–6098.
4. Pyayt, A. L.; Wiley, B.; Xia, Y.; Chen, A.; Dalton, L. Integration of Photonic and Silver Nanowire Plasmonic Waveguides. *Nat. Nanotechnol.* **2008**, *3*, 660–665.
5. Chang, D. E.; Sorensen, A. S.; Demler, E. A.; Lukin, M. D. A Single-Photon Transistor Using Nanoscale Surface Plasmons. *Nat. Phys.* **2007**, *3*, 807–812.
6. Sanders, A. W.; Routenberg, D. A.; Wiley, B. J.; Xia, Y.; Dufresne, E. R.; Reed, M. A. Observation of Plasmon Propagation, Redirection, and Fan-Out in Silver Nanowires. *Nano Lett.* **2006**, *6*, 1822–1826.
7. Yan, R.; Pausauskie, P.; Huang, J.; Yang, P. Direct Photonic–Plasmonic Coupling and Routing in Single Nanowires. *Proc. Natl. Acad. Sci. U.S.A.* **2009**, *106*, 21045–21050.
8. Fang, Y.; Li, Z.; Huang, Y.; Zhang, S.; Nordlander, P.; Halas, N. J.; Xu, H. Branched Silver Nanowires as Controllable Plasmon Routers. *Nano Lett.* **2010**, *10*, 1950–1954.
9. Wei, H.; Li, Z.; Tian, X.; Wang, Z.; Cong, F.; Liu, N.; Zhang, S.; Nordlander, P.; Halas, N. J.; Xu, H. Quantum Dot-Based Local Field Imaging Reveals Plasmon-Based Interferometric Logic in Silver Nanowire Networks. *Nano Lett.* **2011**, *11*, 471–475.
10. Chen, X.-W.; Sandoghdar, V.; Agio, M. Highly Efficient Interfacing of Guided Plasmons and Photons in Nanowires. *Nano Lett.* **2009**, *9*, 3756–3761.
11. Ditlbacher, H.; Hohenau, A.; Wagner, D.; Kreibig, U.; Rogers, M.; Hofer, F.; Aussenegg, F. R.; Krenn, J. R. Silver Nanowires as Surface Plasmon Resonators. *Phys. Rev. Lett.* **2005**, *95*, 257403.
12. Knight, M. W.; Grady, N. K.; Bardhan, R.; Hao, F.; Nordlander, P.; Halas, N. J. Nanoparticle-Mediated Coupling of Light into a Nanowire. *Nano Lett.* **2007**, *7*, 2346–2350.
13. Fang, Z.; Lu, Y.; Fan, L.; Lin, C.; Zhu, X. Surface Plasmon Polariton Enhancement in Silver Nanowire–Nanoantenna Structure. *Plasmonics* **2010**, *5*, 57–62.
14. Fang, Z.; Fan, L.; Lin, C.; Zhang, D.; Meixner, A. J.; Zhu, X. Plasmonic Coupling of Bow Tie Antennas with Ag Nanowire. *Nano Lett.* **2011**, *11*, 1676–1680.
15. Akimov, A. V.; Mukherjee, A.; Yu, C. L.; Chang, D. E.; Zibrov, A. S.; Hemmer, P. R.; Park, H.; Lukin, M. D. Generation of Single Optical Plasmons in Metallic Nanowires Coupled to Quantum Dots. *Nature* **2007**, *450*, 402–406.
16. Wei, H.; Ratchford, D.; Li, X. E.; Xu, H.; Shih, C.-K. Propagating Surface Plasmon Induced Photon Emission from Quantum Dots. *Nano Lett.* **2009**, *9*, 4168–4171.
17. Li, Z.; Bao, K.; Fang, Y.; Huang, Y.; Nordlander, P.; Xu, H. Correlation between Incident and Emission Polarization in Nanowire Surface Plasmon Waveguides. *Nano Lett.* **2010**, *10*, 1831–1835.
18. Li, Z.; Hao, F.; Huang, Y.; Fang, Y.; Nordlander, P.; Xu, H. Directional Light Emission from Propagating Surface Plasmons of Silver Nanowires. *Nano Lett.* **2009**, *9*, 4383–4386.
19. Shegai, T.; Miljkovic', V. D.; Bao, K.; Xu, H.; Nordlander, P.; Johansson, P.; Käll, M. Unidirectional Broadband Light Emission from Supported Plasmonic Nanowires. *Nano Lett.* **2011**, *11*, 706–711.
20. Graff, A.; Wagner, D.; Ditlbacher, H.; Xu, H.; Kreibig, U. Silver Nanowires. *Eur. Phys. J. D* **2005**, *34*, 263–269.
21. Dorfmüller, J.; Vogelgesang, R.; Khunsin, W.; Rockstuhl, C.; Etrich, C.; Kern, K. Plasmonic Nanowire Antennas: Experiment, Simulation, and Theory. *Nano Lett.* **2010**, *10*, 3596–3603.
22. Douillard, L.; Charra, F.; Korczak, Z.; Bachelot, R.; Kostcheev, S.; Lerondel, G.; Adam, P.-M.; Royer, P. Short Range Plasmon Resonators Probed by Photoemission Electron Microscopy. *Nano Lett.* **2008**, *8*, 935–940.
23. Solis, D.; Chang, W.-S.; Khanal, B. P.; Bao, K.; Nordlander, P.; Zubarev, E. R.; Link, S. Bleach-Imaged Plasmon Propagation (BIIPP) in Single Gold Nanowires. *Nano Lett.* **2010**, *10*, 3482–3485.
24. Zou, C.-L.; Sun, F.-W.; Xiao, Y.-F.; Dong, C.-H.; Chen, X.-D.; Cui, J.-M.; Gong, Q.; Han, Z.-F.; Guo, G.-C. Plasmon Modes of Silver Nanowire on a Silica Substrate. *Appl. Phys. Lett.* **2010**, *97*, 183102.
25. Hecht, B.; Bielefeldt, H.; Novotny, L.; Inouye, Y.; Pohl, D. W. Local Excitation, Scattering, and Interference of Surface Plasmons. *Phys. Rev. Lett.* **1996**, *77*, 1889.
26. Bouhelier, A.; Huser, T.; Tamaru, H.; Güntherodt, H.-J.; Pohl, D. W. Plasmon Transmissivity and Reflectivity of Narrow Grooves in a Silver Film. *J. Microsc.* **1999**, *194*, 571.
27. Drezet, A.; Hohenau, A.; Koller, D.; Stepanov, A.; Ditlbacher, H.; Aussenegg, B. S.; Leitner, F.; Krenn, A. J. Leakage Radiation Microscopy of Surface Plasmon Polaritons. *Mater. Sci. Eng., B* **2008**, *148*, 220–229.
28. Bouhelier, A.; Wiederrecht, G. P. Surface Plasmon Rainbow Jet. *Opt. Lett.* **2005**, *30*, 884.
29. Massenot, S.; Grandidier, J.; Bouhelier, A.; Colas des Francs, G.; Markey, L.; Weeber, J.-C.; Dereux, A.; Renger, J.; Gonzàlez, M. U.; Quidant, R. Polymer–Metal Waveguides Characterization by Fourier Plane Leakage Radiation Microscopy. *Appl. Phys. Lett.* **2007**, *91*, 243102.
30. Berthelot, J.; Bouhelier, A.; des Francs, G. C.; Weeber, J.-C.; Dereux, A. Excitation of a One-Dimensional Evanescent Wave by Conical Edge Diffraction of Surface Plasmon. *Opt. Express* **2011**, *19*, 5303–5312.
31. Sun, Y.; Mayers, B.; Herricks, T.; Xia, Y. Polyol Synthesis of Uniform Silver Nanowires: A Plausible Growth Mechanism and the Supporting Evidence. *Nano Lett.* **2003**, *3*, 955–960.
32. Sharma, J.; Vivek, J. P.; Vijayamohanan, K. P. Electron Transfer Behavior of Monolayer Protected Nanoclusters and Nanowires of Silver and Gold. *J. Nanosci. Nanotechnol.* **2006**, *6*, 3464–3469.
33. Colas des Francs, G.; Grandidier, J.; Massenot, S.; Bouhelier, A.; Weeber, J.-C.; Dereux, A. Integrated Plasmonic Waveguides: A Mode Solver Based on Density of States Formulation. *Phys. Rev. B* **2009**, *80*, 115419.
34. Colas des Francs, G.; Hugonin, J.-P.; čtyroký, J. Mode Solvers for Thin Long-Range Plasmonics Waveguides. *Opt. Quantum Electron.* **2010**, *42*, 1–14.
35. Jung, J.; Sondergaard, T.; Bozhevolnyi, S. Theoretical Analysis of Square Surface Plasmon–Polariton Waveguides for Long-Range Polarization-Independent Waveguiding. *Phys. Rev. B* **2007**, *76*, 035434.
36. Johnson, P.; Christy, R. Optical Constants of the Noble Metals. *Phys. Rev. B* **1972**, *6*, 4370.